RSC Advances

PAPER

View Article Online
View Journal | View Issue

Cite this: *RSC Adv.*, 2022, **12**, 8256

Synthesis of chitosan/TCN nanocomposites with the carbon dioxide assisted phase inversion

Binqing Zhao,[ab] Chenxi Lou,[ab] Qi Zhou,[*b] Yating Zhu,[b] Wei Li[ac] and Mu Jingshan*[a]

The chitosan (CS)/bis(2-hydroxyethyl)methyl tallow ammonium modified montmorillonite (TCN) nanocomposites are synthesized by the phase inversion procedure *via* the assistance of carbon dioxide (CO_2). The viscosity of CS/formic acid solution is reduced with the incorporation of CO_2 owing to the formation of carbamic acid. However, the incorporation of TCN promotes the viscosity of CS solution due to the interaction between TCN and carbamic acid. The morphology of CS/TCN nanocomposites is studied by scanning electron microscopy (SEM), where the surface of the membrane is dense and non-porous. The microstructure of the synthesized CS/TCN composite is further investigated by attenuated total reflectance Fourier transform infrared (ATR-FTIR) spectra, X-ray diffraction (XRD), differential scanning calorimetry (DSC), and transmission electron microscopy (TEM). It is found that the incorporation of TCN without the presence of CO_2 disturbs the crystallization of CS. Interestingly, the melting enthalpy of the CS/TCN composite is notably increased with the introduction of CO_2, demonstrating that the interaction between the TCN and carbamic acid enhances the formation of CS crystals. XRD and TEM results show that this interaction is able to promote the homogeneous distribution of TCN in the nanoscale with the non-exfoliated form, enhancing the mechanical properties of the synthesized nanocomposites. In particular, the synthesized CS/TCN nanocomposites with the assistance of CO_2 present exceptional mechanical properties, where the tensile strength (65.82 MPa) and Young's modulus (3512.48 MPa) are twice as high as that of the CO_2 free system.

Received 15th January 2022
Accepted 9th March 2022

DOI: 10.1039/d2ra00296e

rsc.li/rsc-advances

1. Introduction

Chitosan (CS), is a polysaccharide derived from *N*-deacetylation of chitin, and is the most abundant natural polymer besides cellulose (see the schematic structure in Fig. 1a).[1–3] CS exhibits versatile usage because of its biodegradability, chelating properties, film-forming characteristics, antibacterial ability and so on.[4–6] Inorganic fillers, such as carbon nanotubes, polyhedral oligomeric silsesquioxane, SiO_2, *etc.*, are applied to synthesize CS composite materials to improve the chemical and physical properties of CS.[7,8]

Montmorillonite (MMT) is widely studied in polymer composites owing to its tremendous surface area, cation exchange capacity and excellent adsorption ability. Fig. 1b shows the unit layer of methyl tallow ammonium modified montmorillonite (TCN), which consists of two tetrahedral silica sheets and one octahedral aluminum or magnesium sheet. The unit layer shows a net negative charge due to the imperfection of the crystal lattice and isomorphic substitution, which is counterbalanced by bis(2-hydroxyethyl)methyl tallow ammonium cations in the space of the interlayer. TCN also contains –OH groups at the edge of octahedral sheets. The polycationic property of chitosan with abundant –OH and $–NH_2$ groups (*i.e.*, Fig. 1a) is conducive to the dispersion of TCN through intermolecular force like hydrogen bonding.[9,10] Shehap *et al.*[11] prepared high doping CS/MMT nanocomposites for iron removing in water. The intercalation and electrostatic interaction between CS and MMT reinforced the iron removing efficiency of the nanocomposites. Wang *et al.*[12] synthesized novel MMT/CS hydrogels *via* self-assemble of exfoliated MMT nanosheets and CS chains. The hydrogels obtained controllable porous structure and high specific surface area, which allowed their application in sewage treatments, drug carriers and catalyzers. Similarly, the self-assembly procedure was conducted by the hydrogen bonds and electrostatic interaction between electropositive CS and electronegative MMT. Ahmad *et al.*[13] composited MMT/graphene oxide (GO)/CS composite films by a simple solution evaporation method. The MMT/GO/CS films exhibited better thermal stability and mechanical properties. However, the incorporation of plasticizer and freeze-drying process complicated the synthesis procedure.

[a]*School of Material Science and Chemical Engineering, Ningbo University, Ningbo 315211, Zhejiang, P. R. China. E-mail: mujingshan@nbu.edu.cn*

[b]*School of Materials and Chemical Engineering, Ningbo University of Technology, Ningbo 315211, Zhejiang, P. R. China. E-mail: zhouqi@nbut.edu.cn*

[c]*Ningbo Research Institute, Zhejiang University, Ningbo 315100, Zhejiang, P. R. China*

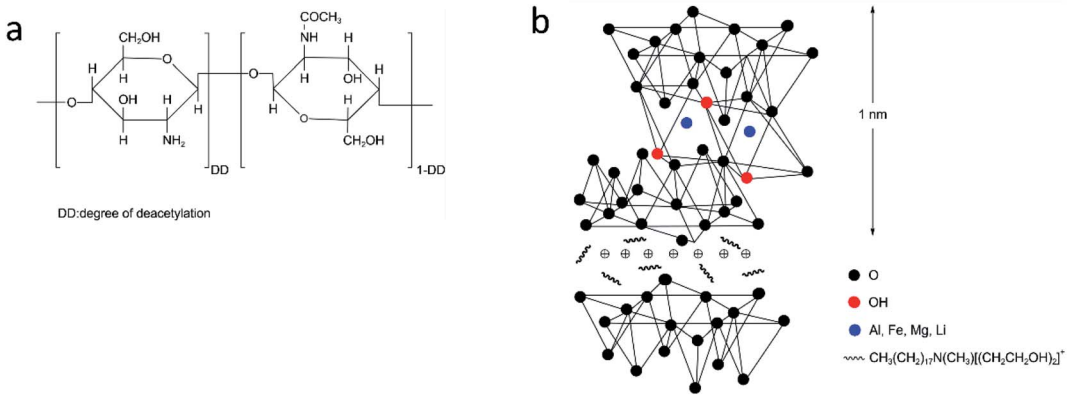

Fig. 1 Structure schematic of (a) chitosan and (b) TCN.

Carbon dioxide (CO_2) is a greenhouse gas which troubles the global climate and human safety for a long time. The emission of CO_2 is generated by industrial processes such as fuel burning and chemical production, which is inevitable in social progress, putting the sustainable and efficacious utilization of CO_2 at a premium.[14,15] Baldino *et al.*[16] investigated supercritical CO_2 assisted phase inversion in producing nanocomposites membranes which conduces in membrane performances. Cardea *et al.*[17] composited nanostructured PVDF–HFP membranes loaded with catalyst obtained by supercritical CO_2 assisted technique and shows a very uniform distribution of catalyst. However, this technique requires high pressure and needs a large energy consumption. Therefore, we attempt to introduce CO_2 into solution directly based on the reaction between amino group and CO_2.[18–20] Mezzetta *et al.*[21] synthesized the cross-linked CS by exploiting CO_2, since the reaction between CO_2 and amino group destructed the hydrogen bonding. Shimoyama *et al.*[22] developed a new dye adsorption technique by CO_2-activated CS, in which the formation of carbamate contributed to the higher dye adsorption capacity and the exceptional removal efficiency.

This work endows a new attempt in the synthesis of CS/bis(2-hydroxyethyl)methyl tallow ammonium modified MMT (TCN) composites through the CO_2 assisted phase inversion. We aim to provide a facial and green method to enhance the mechanical performance of CS/TCN composites. The CO_2 is introduced into the solution to occupy the amino groups of CS chains during the dissolution of CS powder. After the occupation, the exposure of –OH and the deprotonated $–NH_2$ advances the interaction between the TCN and CS chains. Moreover, we find that the tensile strength and Young's modulus of the CS/TCN composites display a significant improvement owning to the improved distribution of TCN.

2. Experimental

2.1 Materials

Chitosan (CS) was purchased from Sinopharm Chemical Reagent Company with the degree of deacetylation > 85%. Bis(2-hydroxyethy)methyl tallow ammonium modified MMT (TCN) was purchased from hybrid plastics company. Formic acid (99%) was purchased from J&K Scientific Ltd. The purity of CO_2 was 99.9%, which was purchased from Fangxin Gas Company, Ningbo.

2.2 Preparation of CS/TCN nanocomposites

0.45 g of CS was dissolved in 45 mL of formic acid under magnetic stirring in a three-necked flask for 8 h. CO_2 was introduced with the access time of 0, 15, 30, 45 min at the beginning of dissolution, respectively. After the complete dissolution of CS, 9 mg of TCN was then added to the CS–CO_2 solution and stirred for 48 h under 600 rpm. After thoroughly mixing, 10 mL of the mixture was transferred to a cell culture dish and kept at 40 °C for 8 h on an electric heating plate (Guohua, DB-4, China). The synthesis scheme is shown in Fig. 2. Samples were placed in a fume hood overnight for volatilization

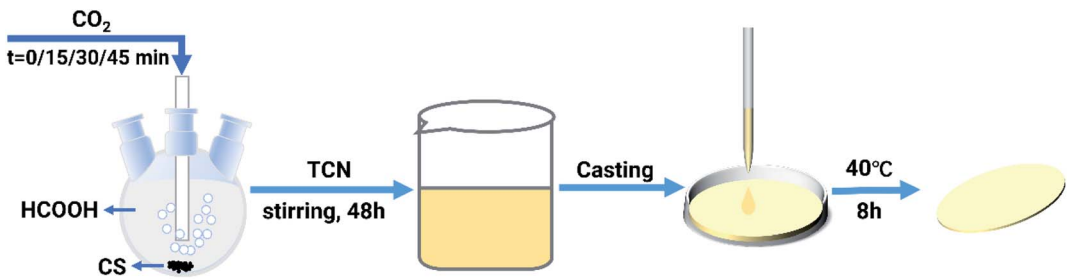

Fig. 2 The synthesis scheme of CS/TCN composites.

of formic acid. The composite film was teared off and soaked in 1% NaOH aqueous solution for 1.5 h and rinse with deionized water until neutral to ensure the absence of formic acid. The composite films were designated as CS-*X*–TCN, where *X* represented the access time of CO_2 ($X = 0$, 15, 30, 45 min, respectively). Membranes were dried in a vacuum oven for 72 h and preserved in a desiccator before using.

2.3 Characterization

Viscosity of CS and CS–TCN solutions were tested by Ubbelohde viscometer in room temperature (25 °C). The results were repeated 3 times and the average value was taken. The conductivity of solution was examined by a conductivity meter (METTLER TOLEDO, Switzerland) at room temperature with a 710 electrode and calibrated with 12.88 mS cm^{-1} conductivity standard. The data was repeated 3 times and the average was taken. The morphology of the membranes was conducted with a scanning electron microscope (SEM, Hitachi S-4800, Japan). The cross section of the membranes was acquired by liquid nitrogen quenching. X-ray diffraction (XRD) measurements were conducted by a Bruker D8 ADVANCE diffract meter at 40 kV and 40 mA ($\lambda = 0.154$ nm) under Cu Kα radiation. The step side and scanning angle was 0.02° and 2°–30°, respectively. The morphology and distribution of TCN nanofillers were characterized by transmission electron microscope (TEM, JEM-1230, Japan). Samples were slit by a frozen section at −120 °C and 70 nm of slice thickness before analysis. Melting point and enthalpy of nanocomposites were detected by differential scanning calorimetry (DSC, Netzsch, DSC 214, Germany) in nitrogen atmosphere at 40 mL min^{-1}. The temperature program was conducted as follows: the samples were heated from 0 °C to 270 °C with the rate of 10 °C min^{-1}. After keeping isothermal for 3 min, the samples were cooled to 0 °C at 10 °C min^{-1}. After waiting for another 3 min at 0 °C, the samples were reheated to 270 °C at 10 °C min^{-1}. The heat fusion during the second heating procedure was recorded. Attenuated total reflectance Fourier transform infrared resonance (ATR-FTIR) analysis was carried out using a Nicolet iS50 spectrometer. The membranes were measured at a resolution of 4 cm^{-1} with a range of 400–4000 cm^{-1} and each spectrum was collected for thirty-two scans. Tensile strength was carried out by universal testing machine (MTS, CMT-4204, United States) equipped with a 100 N tension sensor at 25 °C. Membranes with the width of 10 mm and gauge length of 40 mm were stretched at a crosshead speed of 5 mm min^{-1}. The calculated result was repeated 5 times and the average was taken.

3. Results and discussion

The dependence of CS and CS/TCN solution conductivities on the CO_2 incorporation time is shown in Fig. 3, where a much higher value is shown in the CO_2 modified system. It was demonstrated that the dissolution of CS in formic acid was due to the protonation of amino groups ($-NH_3^+$), which raised the solution conductivity. The conductivity of CS/formic acid solution is reduced in the initial 15 min of CO_2 incorporation, which is in evidence as the formation of carbamic acid (–NHCOOH) by the reaction of CO_2 and $-NH_2$.[21,22] The increased conductivity of CS solution with the further extension of CO_2 incorporation time may lead to the formation of ammonium carbamic salt ($-H_3N^+:{}^-OC(O)NH-$) according to the interaction between –NHCOOH and $-NH_3^+$.[19,20,23] This was evidenced in our previous work, where the *in situ* diffuse reflectance infrared Fourier transform (DRIFT) experiment was utilized to detect and demonstrate the reaction process of CO_2 and CS powder.[24] With the addition of TCN, the conductivities of CS/TCN solutions are decreased with respect to that of the CS solutions. Moreover, the dependence of conductivities on the incorporation time of CO_2 is similar in the CS and CS/TCN solutions. These indicate that TCN can interact with CS through its $-NH_3^+$ groups, thus reduce the solution conductivity.

The viscosity of CS based solutions are further shown in Fig. 3b. The viscosity of CS/formic acid solution is reduced in the initial 15 min of CO_2 incorporation, which is owing to the reduction of $-NH_3^+$. This effect depresses the repulsion effect caused by charged segments and facilitates the movements of CS chains.[21,22] Further incorporation of CO_2 leads to the formation of ammonium carbamic salts, which makes the crosslinking of CS chains.[19,20,23] Upon the incorporation of TCN, the viscosity the CS/TCN solution without CO_2 is smaller than that of the pure CS solution, owing to the interaction of TCN and CS (*i.e.*, $-NH_3^+$) as proved above. Interestingly, with the incorporation of CO_2, the reduction amplitude of solution viscosity becomes small, and the viscosity of TCN system is even higher than that of TCN-free case after 10 min incorporation of

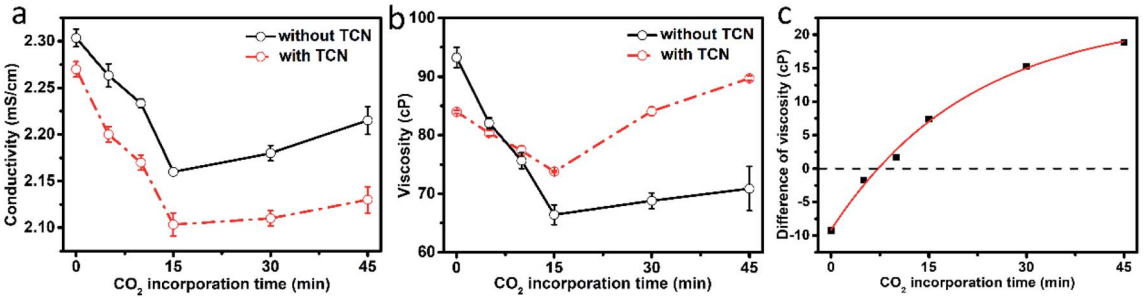

Fig. 3 The properties of CS and CS/TCN solutions on the incorporation time of CO_2 (a) the conductivity of the CS and CS/TCN solutions; (b) viscosity of the CS and CS/TCN solutions; (c) deviation of viscosity upon the incorporation of TCN with respect to the TCN-free system.

CO_2.[26] This indicates that TCN is tend to interact with other groups of CS. The deviation of viscosity upon the incorporation of TCN is calculated with respect to that of the TCN-free system (see Fig. 3c). It is shown that the deviation of CS/TCN solutions is exponentially increased with the increment of CO_2 incorporation time, which is attributed to the interaction between TCN and –NHCOOH group (*i.e.*, the reaction products of CO_2 and CS). However, the –NHCOOH will react with $-NH_2$ of CS with further incorporation of CO_2. This will crosslink the CS chains and limit the interaction between TCN and CS, where the increase rate of viscosity deviation is gradually reduced. Thus, it is demonstrated that the incorporation of CO_2 can promote the interaction between TCN and CS through the newly formed carbamic acid.

The surface morphology of CS/TCN membranes is investigated by SEM (see Fig. 4a–d), in which the surface is smooth, indicating the homogeneous distribution of TCN. In addition, to observe the internal structure of composite films, the cross section morphology was researched in Fig. 4e and f. It is found that there is no agglomeration of filler in matrix. These results indicates that the composite membranes are dense and out of porous.

The X-ray powder diffraction (XRD) patterns of TCN, pure CS and CS/TCN composites synthesized at different CO_2 incorporation time are shown in Fig. 5a. The pure CS displays two diffraction peaks at ~11° and ~21°, which can be ascribed to the intermolecular and intramolecular hydrogen bonds, respectively. The XRD pattern of TCN displays a strong characteristic peak at 5°.[27,28] There is no shift or disappearance of the characteristic peak, which indicates the TCN is not exfoliated in the CS matrix. To get exfoliated MMT sheets in TCN, the pretreatment (*e.g.*, ultrasonication, intercalation polymerization, *etc.*) is essential,[11,29] which is not used in this experiment. Interestingly, compared with the intensity of TCN characteristic peak, the resonance of intermolecular bonding of CS is first decreased and then increased with the incorporation of CO_2, reaching to the minimum at 30 min of CO_2 incorporation (Fig. 5b). This demonstrates that the interaction between the TCN and CS limits the formation of hydrogen bonding generated by the CS intermolecular chains.

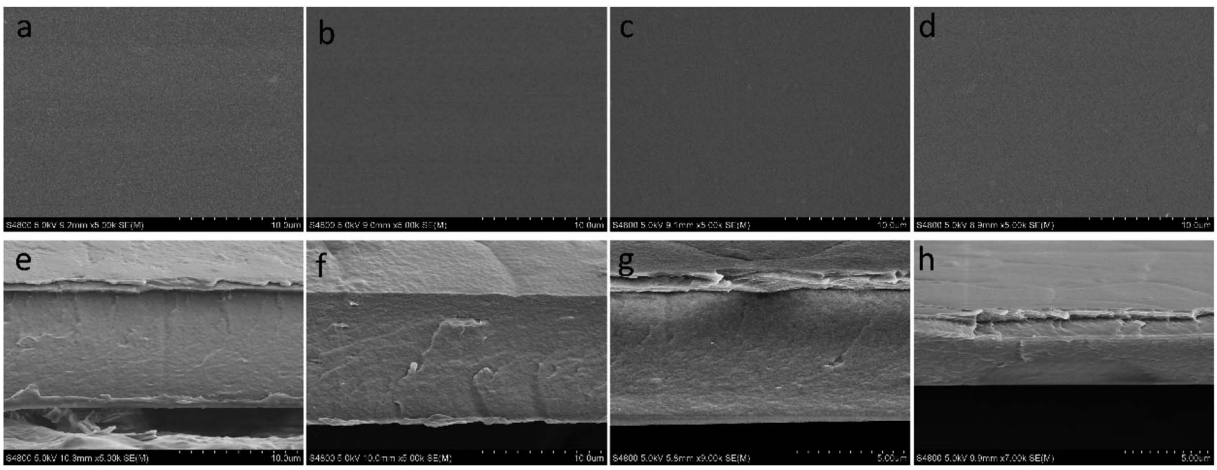

Fig. 4 SEM images of the CS/TCN composites: surface images: (a) CS-0–TCN, (b) CS-15–TCN, (c) CS-30–TCN, (d) CS-45–TCN; cross section images: (e) CS-0–TCN, (f) CS-15–TCN, (g) CS-30–TCN, (h) CS-45–TCN.

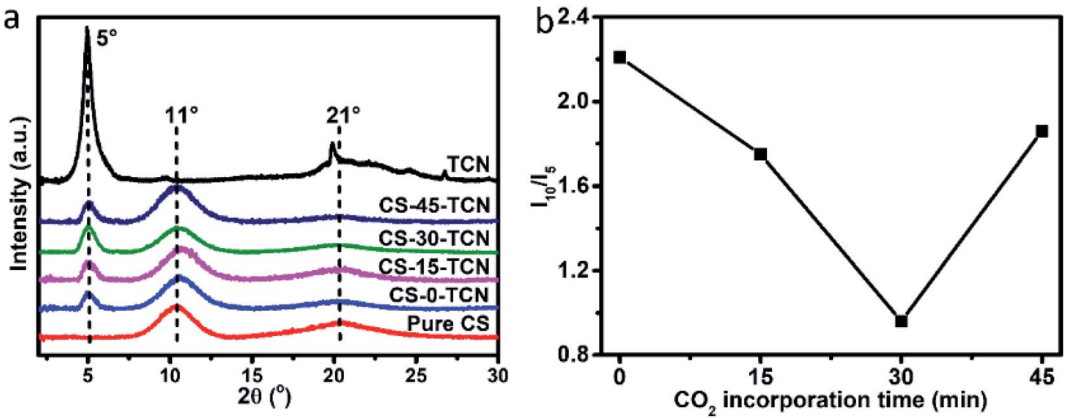

Fig. 5 (a) XRD patterns of TCN, CS and CS/TCN composites; (b) intensity ratio of 10° and 5°.

The ATR-FTIR spectra of CS and CS/TCN membranes are given in Fig. 6 to characterize the variation of molecular structure and bonding environment. The bond around 3300 cm^{-1} corresponds to the N–H and O–H stretching vibration. The peaks at 2917 cm^{-1} and 2874 cm^{-1} can be described to C–H stretching vibration. The peaks at 1670 cm^{-1} and 1587 cm^{-1} represents for C=O stretching vibration and N–H bending vibration, which derive from acetylated and formylated amino groups of CS, respectively. The C–O–C stretching vibration of the ring is detected at 1154 cm^{-1}. The peak at 1076 cm^{-1} comes from secondary –OH of CS.[30–32] In contrast to pure CS, the peak around 3300 cm^{-1} of CS–TCN is declined, indicating the interaction between CS and TCN reduces the hydrogen bonding of CS matrix. Moreover, the intensity of hydrogen bonding has a further decrement with the introducing of CO_2, reaching the minimum at 30 min. The dependence of hydrogen bonding on the CO_2 incorporation time is related to the formation of carbamic acid that facilitate the interaction between TCN and CS.[19,20,25] However, the formation of carbamic salt will hinder the reduction of hydrogen bonding due to the crosslinked CS chains. As a result, the resonance of 3300 cm^{-1} is enhanced backward at much longer time of CO_2 incorporation, where the least intensity of hydrogen bonding is found in the CS-30–TCN.

The effects of TCN and CO_2 on the thermodynamics and crystalline behavior of CS based membranes are shown in Fig. 7. An endothermic peak around 130 °C was observed, presenting the typical melting point of CS.[32,33] With the addition of TCN, the melting enthalpy of CS/TCN is reduced (from 217.6 to 140.4 J g^{-1}), which indicates the incorporation of TCN destroys the crystallization of CS. Interestingly, the melting enthalpy is notably increased with the introduction of CO_2 at 15 min. This indicates the enhanced crystalline behavior of CS/TCN owing to the formation of carbamic acid. These results may be brought by the better dispersion of TCN in CS matrix owing to the interaction between the TCN and the carbamic acid.[27] However, this interaction is blocked with the further increment of CO_2 incorporation time, since the formation of ammonium carbamic salt limits the interaction between CS and TCN.

The TCN distribution in the CS matrix is further evidenced by the TEM images (see Fig. 8), where the TCN fillers are homogeneously distributed in the matrix with the non-exfoliated form. This further evidence that the interlayer of TCN filler is not exfoliated. The filler size in the CS-15–TCN is much less than that

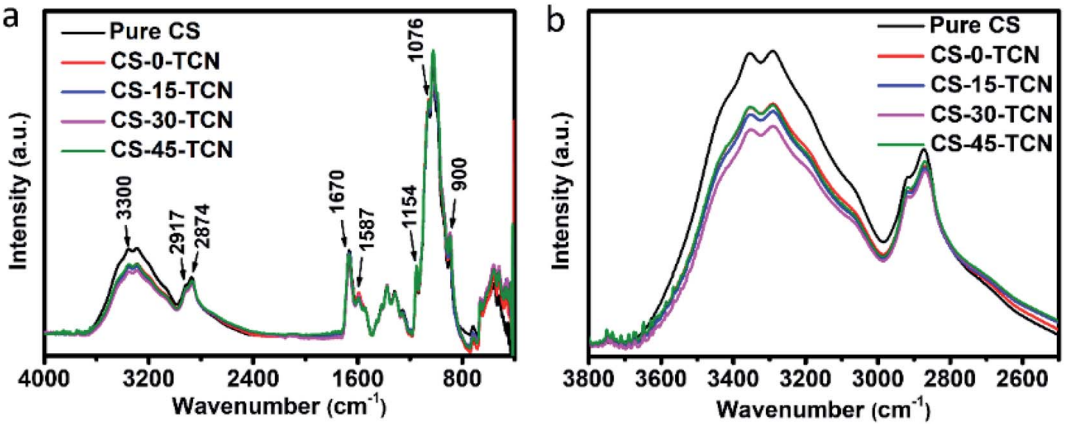

Fig. 6 ATR-FTIR spectra of CS and CS/TCN composites, (a) full ATR-FTIR spectra; (b) the enlarged spectra with the region ranging from 3800 to 2500 cm^{-1}. Pure CS was synthesized in the absence of CO_2.

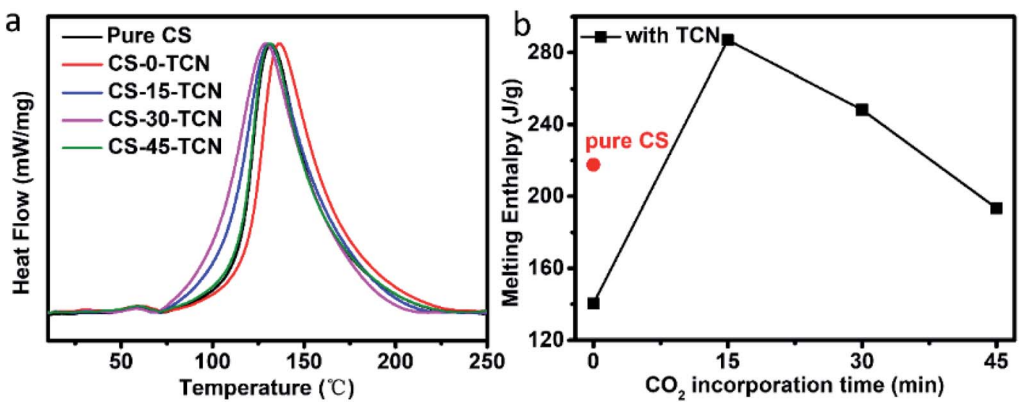

Fig. 7 (a) DSC curves of pure CS and CS/TCN composites; (b) melting enthalpy of pure CS and CS/TCN composites.

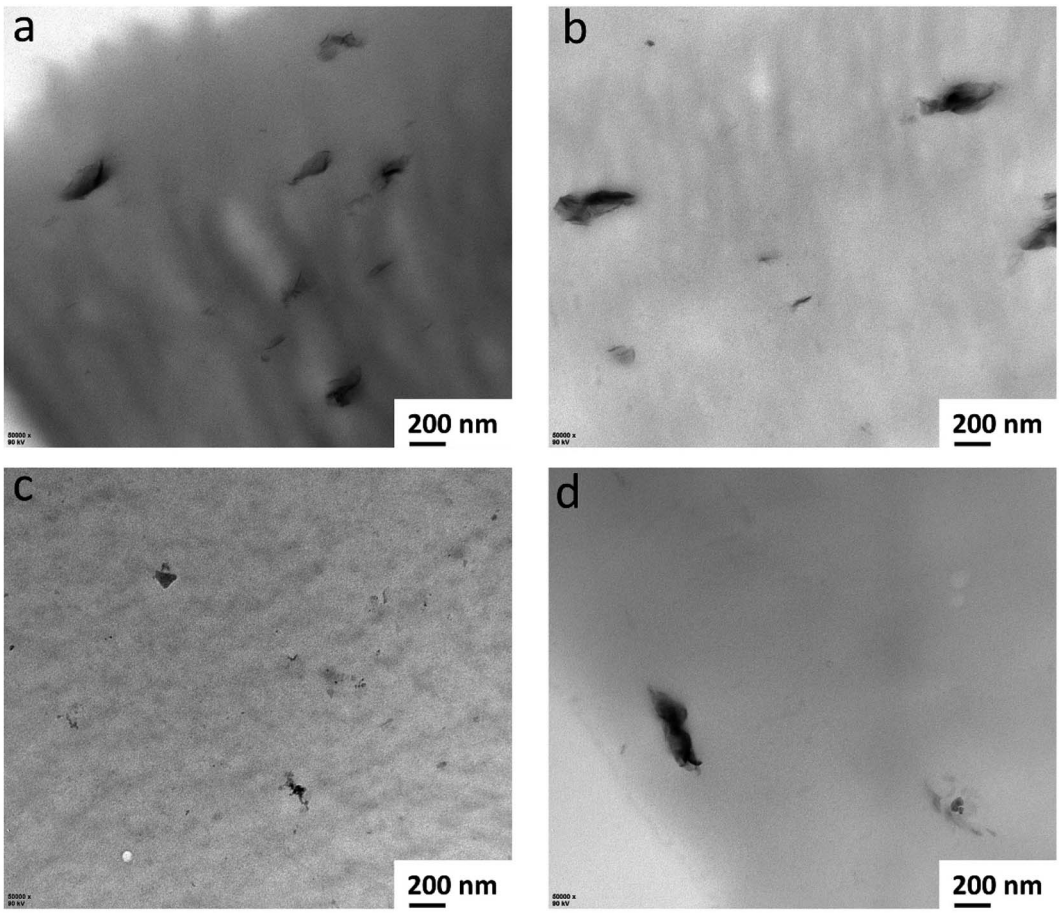

Fig. 8 TEM of the CS/TCN composites: (a) CS-0–TCN, (b) CS-15–TCN, (c) CS-30–TCN, (d) CS-45–TCN.

of the CO_2-free case owing to the incorporation CO_2. This further demonstrates that the improved interaction between CS and TCN facilitates the homogeneous distribution of fillers. However, the dispersion of TCN is deteriorated due to the crosslinking of CS matrix, achieving the most uniformed distribution with the small size of fillers in the CS-30–TCN.[19,20]

Fig. 9 shows the tensile strength (Fig. 9a) and Young's modulus (Fig. 9b) of the composites. The mechanical properties of CS (*i.e.*, tensile strength of 50.62 MPa and Young's modulus of 2306.30 MPa) are declined with the incorporation of TCN, due to the uneven distribution of TCN and the reduced crystallinity. It is observed that the CO_2 modified CS–TCN nanocomposites strengthen the mechanical properties. The formation of carbamic acid facilitates the distribution of fillers and improve the crystalline behavior of CS, causing an exaltation of stress transfer property.[23,34] The maximum of tensile

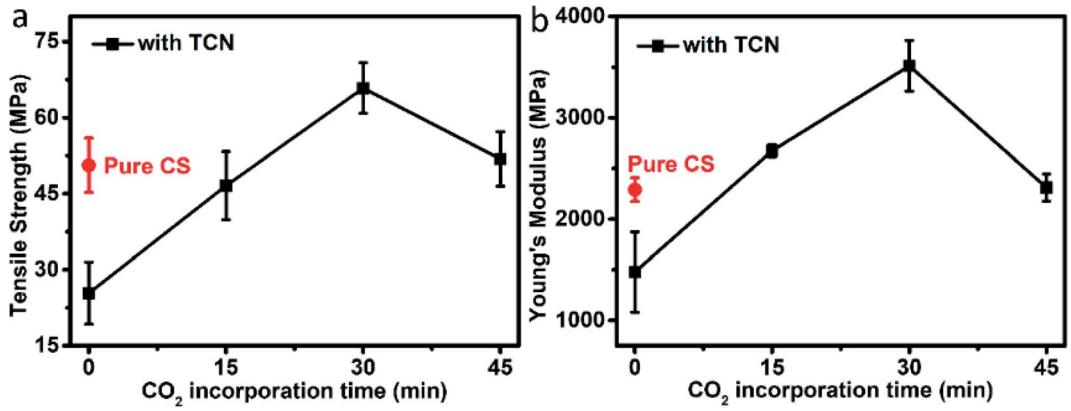

Fig. 9 Mechanical properties of pure CS and CS/TCN composites: (a) tensile strength; (b) Young's modulus.

strength and Young's modulus are shown in CS-30–TCN, owning to the balance between the contribution of filler dispersion and crystalline enhancement.

4. Conclusions

In summary, it has been shown that the synthesis of CS/TCN composites by the CO_2 assisted phase inversion process is an efficient and convenient method in tailoring the filler distribution. The incorporation of CO_2 leads to the formation of carbamic acid along the CS chains, improving the interaction between the TCN and CS. This effect facilitates the dispersion of TCN and the crystalline behavior of CS domains. However, the excessive incorporation of CO_2 leads to the worse distribution of TCN due to the crosslinking of CS chains. Consequently, the CS-30–TCN (*i.e.*, with 30 min of CO_2 feeding) presents the better distribution of TCN with the exceptional melting enthalpy of CS, where the rigidity and strength of the CS/TCN composites are enhanced. Looking forward, it is anticipated that the CO_2 assisted phase inversion procedure will also prove valuable in the synthesis of other CS derivative composites, which provides a green and facile method for the utilization of CO_2.

Conflicts of interest

There are no conflicts to declare.

Acknowledgements

The authors are grateful for the support of the Natural Science Foundation of Zhejiang Province (LY20B060003), and the Key Project of Natural Science Foundation of Ningbo (202003N4017).

References

1 B. H. Morrow, G. F. Payne and J. Shen, *J. Am. Chem. Soc.*, 2015, **137**, 13024–13030.
2 M. A. Pigaleva, I. V. Portnov, A. A. Rudov, I. V. Blagodatskikh, T. E. Grigoriev, M. O. Gallyamov and I. I. Potemkin, *Macromolecules*, 2014, **47**, 5749–5758.
3 T. T. Nhung and S. W. Lee, *ACS Appl. Mater. Interfaces*, 2014, **6**, 21335–21345.
4 S. M. Ahsan, M. Thomas, K. K. Reddy, S. G. Sooraparaju, A. Asthana and I. Bhatnagar, *Int. J. Biol. Macromol.*, 2018, **110**, 97–109.
5 R. Jayakumar, N. New, S. Tokura and H. Tamura, *Int. J. Biol. Macromol.*, 2007, **40**, 175–181.
6 D. Vukajlovic, J. Parker, O. Bretcanu and K. Novakovic, *Mater. Sci. Eng., C*, 2019, **96**, 955–967.
7 R. Zhiani, A. Es-haghi, F. Shamsa, F. Amarloo, M. Shahroudi and S. M. Sadeghzadeh, *Silicon*, 2020, **12**, 2005–2015.
8 S. F. Wang, L. Shen, W. D. Zhang and Y. J. Tong, *Biomacromolecules*, 2005, **6**, 3067–3072.
9 M. Darder, M. Colilla and E. Ruiz-Hitzky, *Chem. Mater.*, 2003, **15**, 3774–3780.
10 F. Chivrac, E. Pollet and L. Avérous, *Mater. Sci. Eng., R*, 2009, **67**, 1–17.
11 A. M. Shehap, R. A. Nasr, M. A. Mahfouz and A. M. Ismail, *J. Environ. Chem. Eng.*, 2021, **9**, 104700.
12 W. Wang, Y. Zhao, H. Yi, T. Chen, S. Kang, H. Li and S. Song, *Nanotechnology*, 2018, **29**, 025605.
13 M. Yadav and S. Ahmad, *Int. J. Biol. Macromol.*, 2015, **79**, 923–933.
14 J. Chen, J. Yang, G. S. Hu, X. Hu, Z. M. Li, S. W. Shen, M. Radosz and M. H. Fan, *ACS Sustainable Chem. Eng.*, 2016, **4**, 1439–1445.
15 Y. Y. Zhan, Q. Q. Han, S. F. Pan, X. Kan, J. X. Mi, F. J. Liu, Y. N. Cao, C. Au and L. L. Jiang, *Ind. Eng. Chem. Res.*, 2019, **58**, 7980–7988.
16 L. Baldino, J. Aragón, G. Mendoza, S. Irusta, S. Cardea and E. Reverchon, *J. Chem. Technol. Biotechnol.*, 2019, **94**, 98–108.
17 S. Cardea and E. Reverchon, *Chem. Eng. Process.*, 2011, **50**, 630–636.
18 E. M. Hampe and D. M. Rudkevich, *Tetrahedron*, 2003, **59**, 9619–9625.
19 S. Stegmeier, M. Fleischer, A. Tawil, P. Hauptmann, K. Egly and K. Rose, *Procedia Chem.*, 2009, **1**, 236–239.
20 V. Stastny and D. M. Rudkevich, *J. Am. Chem. Soc.*, 2007, **129**, 1018–1019.
21 A. Mezzetta, L. Guazzelli and C. Chiappe, *Green Chem.*, 2017, **5**, 1235–1239.
22 H. Q. Le, Y. Sekiguchi, D. Ardiyanta and Y. Shimoyama, *ACS Omega*, 2018, **3**, 14103–14110.
23 D. Nagai, A. Suzuki, Y. Maki and H. Takeno, *Chem. Commun.*, 2011, **47**, 8856–8858.
24 B. Q. Zhao, Q. Zhou, C. X. Lou, X. P. Jin and W. Li, *Int. J. Biol. Macromol.*, 2021, **193**, 287–292.
25 S. H. Chang and M. H. Hsieh, *Polym. Polym. Compos.*, 2021, **29**, 1442–1449.
26 M. A. Pigaleva, I. V. Portnov, A. A. Rudov, I. V. Blagodatskikh, T. E. Grigoriev, M. O. Gallyamov and I. I. Potemkin, *Macromolecules*, 2014, **47**, 5749–5758.
27 Q. Zhou, J. Y. Zhang, J. H. Fang and W. Li, *RSC Adv.*, 2015, **5**, 16631–16639.
28 Q. Zhou, J. J. Zhang, T. Saba, Z. Yue, W. Li, J. A. Anderson and X. D. Wang, *ACS Sustainable Chem. Eng.*, 2019, **1**, 1271–1278.
29 L. Jiankun, Y. Ke, Z. N. Qi and X. Yi, *J. Polym. Sci., Part B: Polym. Phys.*, 2001, **39**, 115–120.
30 R. T. De Silva, M. G. P. Mantilaka, S. P. Ratnayake, G. A. J. Amaratunga and K. M. N. De Silva, *Carbohydr. Polym.*, 2017, **157**, 739–747.
31 J. Madejová, *Vib. Spectrosc.*, 2003, **31**, 1–10.
32 A. Zając, J. Hanuza, M. Wandas and L. Dymińska, *Spectrochim. Acta, Part A*, 2015, **134**, 114–120.
33 Y. Dong, Y. H. Ruan, H. W. Wang, Y. G. Zhao and D. X. Bi, *J. Appl. Polym. Sci.*, 2004, **93**, 1553–1558.
34 K. Sakurai, T. Maegawa and T. Takahashi, *Polymer*, 2000, **41**, 7051–7056.